


Spatially Modulated Superfluid State in Two-Dimensional ^4He Films

Jaewon Choi,^{†,§} Alexey A. Zadorozhko,^{‡,§} Jeakyung Choi[✉], and Eunseong Kim^{*}
*Department of Physics, Korea Advanced Institute of Science and Technology (KAIST),
 291 Daehak-ro, Yuseong-gu, Daejeon 34141, Republic of Korea*

 (Received 24 March 2021; accepted 30 July 2021; published 21 September 2021)

The second layer of ^4He films adsorbed on a graphite substrate is an excellent experimental platform to study the interplay between superfluid and structural orders. Here, we report a rigid two-frequency torsional oscillator study on the second layer as a function of temperature and ^4He atomic density. For the first time, we show experimentally that the superfluid density is independent of frequency, which can be interpreted as unequivocal evidence of genuine superfluidity. The phase diagram established in this work reveals that a superfluid phase coexists with hexatic density-wave correlation and a registered solid phase. This suggests the second layer as a candidate for hosting two exotic quantum ground states: the spatially modulated superfluid and supersolid phases resulting from the interplay between superfluid and structural orders.

DOI: 10.1103/PhysRevLett.127.135301

Interplay among different orders is a hallmark of correlated quantum systems [1–3]. High-temperature superconductors [4–6], heavy-fermion compounds [7,8], and low-dimensional materials [9–11] have been studied as model systems, where multiple broken-symmetry phases are intertwined and exotic quantum phases emerge. Similarly, each layer of ^4He films adsorbed on graphite substrates allows for the realization of exotic quantum phenomena in a two-dimensional system, subject to periodic triangular potential. For example, the first layer undergoes successive structural transitions due to strong substrate potential [12,13]. Superfluidity found in the third layer is an experimental manifestation of the Berezinskii-Kosterlitz-Thouless (BKT) phase transition [14–16].

In the second layer, a delicate balance between ^4He - ^4He and ^4He -graphite interactions plays a significant role. The second layer has accordingly been widely studied as a candidate for hosting a supersolid ground state in which both long-ranged superfluid and solid orders coexist in a single homogeneous phase. Indeed, superfluidity was reported in torsional oscillator (TO) experiments [16–18] near the ^4He atomic density (or coverage) where the signature of a solid melting in the heat capacity was observed [19–21] and the existence of a commensurate solid phase has been predicted [22–24]. The unusual $\log(T)$ behavior and the absence of a sharp onset in the previous TO experiments cannot be understood in the framework of BKT theory alone. Recently, it was suggested that the intertwined superfluid and density-wave orders lead to a sixfold softening of the rotonlike mode, which explains the lack of BKT transition [18,25]. Thus, the strong interplay between the superfluid and structural orders may be the key to understanding the exotic superfluid behaviors and exploring the possible supersolid phase in the second layer.

However, two outstanding questions still remain to be addressed: First, can we attribute the TO responses to the emergence of superfluidity? Since the oscillating motion of TOs can also be influenced by mechanisms other than superfluidity [26], experiments that disentangle the superfluid contribution from that of nonsuperfluid origins are necessary. Second, do the superfluid and structural orders coexist in a common coverage range or lie in separate coverage regions? It would be interesting to understand their relationship, if they indeed coexist.

Here, we present a two-frequency TO study on the second layer of ^4He films adsorbed on graphite to address the above-mentioned questions. The superfluid density ρ_s is measured as a function of temperature and coverage. ρ_s measured at two different frequencies are equivalent, indicating that the TO responses can be credited to genuine superfluid transition. By *in situ* pressure measurement, the phase diagram for the second layer is more accurately determined and compared to other studies. The superfluid phase emerges in the liquid region where the superfluid order with hexatic density correlation was predicted [24]. The superfluid order is rapidly suppressed in the region where both superfluid and registered solid phase coexist, revealing a competing relationship between them. This coexistence region can be interpreted as a candidate for the long-sought supersolid phase.

For unambiguous detection of the superfluid phase, a rigid two-frequency TO containing a Grafoil substrate was fabricated [Fig. 1(a)]. Unlike conventional single-mode TOs [16–18], it measures ρ_s at two different frequencies: 511 Hz (low mode, f_-) and 1246 Hz (high mode, f_+), with a quality factor of 10^6 . An *in situ* diaphragm-type pressure gauge was installed to measure the vapor pressure of the ^4He films. Figure 1(b) shows the N_2 pressure isotherm of

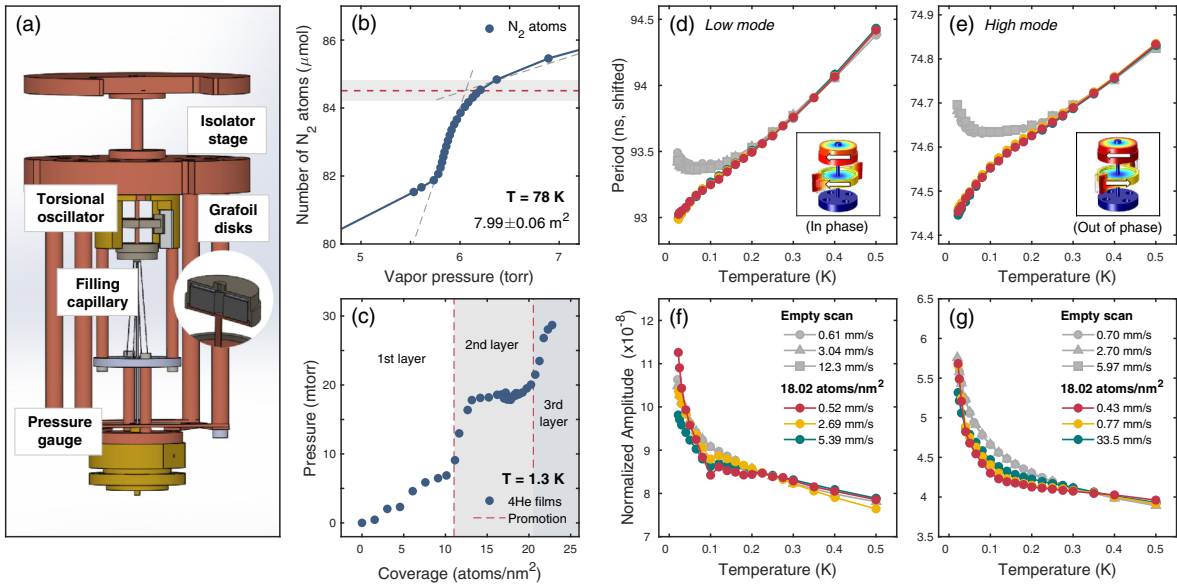


FIG. 1. Superfluid measurement in two-dimensional ^4He films. (a) Rigid two-frequency torsional oscillator (TO). (b) N_2 pressure isotherm for the determination of the surface area of substrate. (c) Layer-by-layer growth of ^4He films manifested by discontinuous increases in vapor pressure. (d),(e) Temperature dependence of the TO period, and (f),(g) amplitude in the low (in-phase) and high (out-of-phase) modes at different rim velocities. Empty TO responses (gray symbols) obtained at different driving velocities are superimposed over each other, indicating that the TO operates in the linear response regime.

the Grafoil substrate determining its surface area. Because of the completion of the $\sqrt{3} \times \sqrt{3}$ commensurate solid phase at 6.37 atoms/nm^2 [27], the slope changes suddenly at $8.45 \times 10^{-5} \text{ mol}$ corresponding to $7.99 \pm 0.06 \text{ m}^2$. Ultrapure ^4He gas with a ^3He impurity concentration of 0.6 ppb was systematically dosed to the sample cell and annealed at high temperatures. We confirm the layer-by-layer growth [28,29] via the ^4He vapor pressure isotherm [Fig. 1(c)] that shows two clear jumps at 11.1 and 20.4 atoms/nm^2 (see Fig. 1 in the Supplemental Material [30]).

Figures 1(d)–1(g) show the typical temperature dependence of the TO period and amplitude, measured at a ^4He atomic density n (or coverage) of 18 atoms/nm^2 . In both modes, the period deviates from that of the empty TO at the onset temperature $T_s \sim 250 \text{ mK}$ upon cooling [Figs. 1(d) and 1(e)]. Our TO was specifically designed to distinguish the physical origin of this period reduction, δP_{\pm} . If part of the ^4He films undergoes a superfluid transition below T_c , it decouples from the oscillation of the TO and hence does not contribute to the rotational inertia of ^4He . This “missing” inertia leads to a decrease in the resonant period of the TO, δP_{\pm} . The superfluid density $\rho_s(T, n)$ is then determined independent of frequency by $\rho_s = \delta P_{-}(T, n) / \Delta P_{-}(n) = \delta P_{+}(T, n) / \Delta P_{+}(n)$, where $\Delta P_{\pm}(n)$ is the period increase at 500 mK due to the ^4He mass added to the second layer. Other mechanisms such as viscoelastic property change [26,31] or slippage of ^4He atoms on the substrate [32,33], on the other hand, produce nontrivial frequency responses. For example, the viscoelastic

stiffening of solid ^4He induces a superfluid-mimicking period reduction $\delta P / \Delta P$ proportional to f^2 , virtually indistinguishable from genuine superfluid transition by single-mode TOs [26]. The TO amplitude shows a broad dip in the temperature range where the period reduction appears [Figs. 1(f) and 1(g)]. The period curve remains unaffected upon increased oscillation speeds; thus, the superfluid critical velocity v_c exceeds 33 mm/s, consistent with that of ^4He films [34].

Figure 2 shows $\rho_s(T)$ measured at various coverages in the second layer. We first observe ρ_s above our detection limit at $n_c = 17 \text{ atoms/nm}^2$. A TO period and amplitude below n_c are superimposed with a vertically shifted empty-TO background (see Fig. 2 in the Supplemental Material [30]). The absence of a “tilted” or “composite” background [35,36] confirms that our TO adopting rigid design principle is unaffected by the complicated viscoelastic coupling between the ^4He films and TO body observed in other nonrigid TOs [16–18]. As n increases to 18.23 atoms/nm^2 , ρ_s reaches its maximum value of $\sim 0.9\%$. Above this coverage, ρ_s is rapidly suppressed and disappears at 18.83 atoms/nm^2 . Remarkably, the ρ_s measured at two different frequencies are essentially identical. This observation of a frequency-independent ρ_s can be interpreted as distinctive evidence of genuine superfluidity in the second layer. This conclusion is supported by TO responses of BKT superfluid in the third layer (see Fig. 3 in the Supplemental Material [30]) [16,17]. We also find ρ_s to be frequency-independent in the third layer, confirming our rationale.

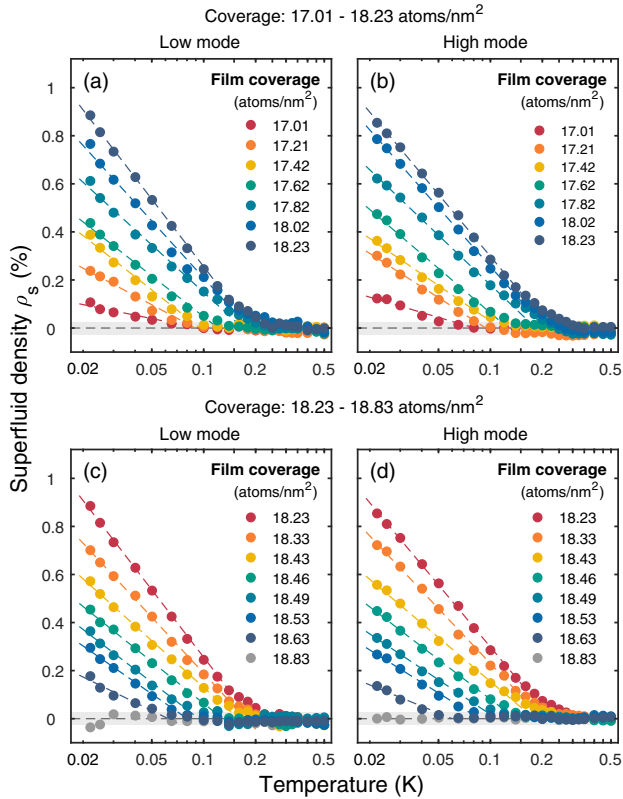


FIG. 2. Temperature evolution of second layer superfluidity. Superfluid density ρ_s as a function of temperature T in a coverage region of 17.01–18.23 atoms/nm² for the (a) low- and (b) high-frequency modes, and 18.23–18.83 atoms/nm² for the (c) low- and (d) high-frequency modes. The dashed lines are linear fits of ρ_s as a function of $\log(T)$.

Besides the frequency-independent ρ_s , there are a few more remarkable features of the second layer superfluidity. First, the temperature evolution of ρ_s is much slower than that expected from the BKT theory. This theory predicts a sudden increase in $\rho_s(T)$ at the onset temperature due to vortex-antivortex unbinding, followed by shallow phonon-like excitation with T^3 dependence at low temperature [37]. However, $\rho_s(T)$ measured in the second layer increases proportionally to $\log(T)$ in both frequencies (Fig. 2). This trend is in stark contrast to the superfluid behavior in the third layer, where a typical broadened BKT transition was observed (see Fig. 3 in the Supplemental Material [30]). This $\rho_s \sim \log(T)$ with the slow onset has also been reported in previous TO experiments [16–18]. Such unusual behavior was recently attributed to intertwined superfluid and density-wave orders and has been associated with a softening of the rotonlike modes [18] or a “failed” superfluid in absence of topologically stable vortices due to spatial modulation [25]. Second, ρ_s does not strongly depend on the ³He impurity concentration. Although we used ultrahigh-purity ⁴He gas with 0.6 ppb ³He impurities several orders of magnitude smaller than other studies [16,17], similar ρ_s and T_s are observed. Therefore, ³He impurity

does not lead to significant effects on the superfluid transition in the second layer. It is notable that the robust superfluidity at (or immunity to) the extremely low concentration of ³He is a typical characteristic of a BKT superfluid. Third, $\rho_s \sim 0.9\%$ can be understood by the tortuosity effect with $\chi \sim 0.98$, measured near the third-layer completion. This indicates that a significant fraction of ⁴He atoms in the second layer participate in the superflow. Although $\rho_s(T)$ resembles the slow onset reported in the TO response in bulk solid ⁴He, the present observations of frequency independence, weak ³He dependence, and high critical velocity are interpreted as unequivocal evidence of superfluidity in the second layer.

In Figs. 3(a) and 3(b), we map out $\rho_s(T, n)$ in the second layer at both frequencies. The white dashed lines are the contours of ρ_s . The maps reconfirm the frequency independence of the superfluid over the entire parameter space. The superfluid onset T_s determined in Fig. 4 of the Supplemental Material [30] is plotted in Fig. 3(c) against n . Until n reaches ~ 17.6 atoms/nm², $T_s(n)$ increases slowly. Above this value, $T_s(n)$ grows much faster, following a linear function of n , $T_s(n) \sim 0.15(n - n_0)$ where $n_0 = 16.8$ atoms/nm² is the coverage of an inert layer. This slope is consistent with both third-layer superfluid and superfluid films adsorbed on mylar [38], which are well understood by the BKT phase transition. The similarity between the second and third layers further suggests that the observed superfluid responses are associated with the same region of the Grafoil substrate. If they stem from different regions—for example, one in the crests between crystallites and the other on the crystalline surface, the slope of $T_s(n)$ should be different due to the different areal densities. In addition, the ρ_s isotherm at 22 mK is shown in Fig. 3(d). The BKT relation $\rho_s/T_s = 8\pi k_B m^2/h^2$ predicts that T_s is linearly proportional to ρ_s . Figure 3(e) demonstrates that the second layer superfluid on graphite satisfies the linear relation, which has been found in ⁴He films on various substrates [39]. This implies that the superfluid phase in the second layer might not be entirely distinct from the BKT superfluid found above the third layer, although strong interplay with structural order suppresses its sharp onset.

Simultaneous TO and *in situ* vapor pressure measurements enable us to determine an accurate coverage scale. Based on this, we propose an $n - T$ phase diagram of the second layer in Fig. 4. To reconcile with different experiments, we introduce a “reduced” coverage $n_r = n/n_2$, where n_2 is the coverage for second layer completion. The superfluid onset $T_s(n)$ measured in this work is plotted with cyan symbols. Previously, three structural phases have been identified by heat capacity measurements [19–21]; we incorporate the results applying our reduced coverage scale into the proposed phase diagram. The low-density region is assigned to a gas-liquid coexistence (GL) phase, evidenced by heat capacity peaks near 0.8 K nearly independent of n .

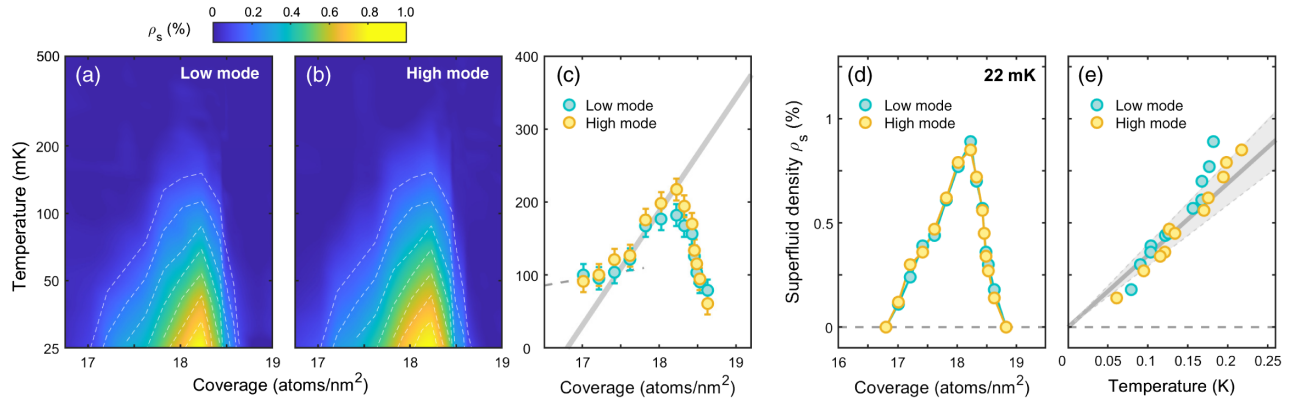


FIG. 3. Coverage dependence of the second layer superfluidity. False-color map of superfluid density ρ_s in the second layer as a function of coverage n and temperature T measured at (a) the in-phase and (b) the out-of-phase modes. The dashed lines are contours of ρ_s from 0.1 (outermost) to 0.7 (innermost) with a step of 0.1. (c) Superfluid onset temperature T_s as a function of n . The gray solid line is the prediction from BKT theory $T_c(n) = 0.15(n - n_0)$ [38]. (d) ρ_s isotherm at 22 mK plotted against n . (e) Testing the linear relation between ρ_s and T_s . The solid gray line is a linear fit fixing the y intercept to zero. The shaded region indicates 1 σ bound (or 68% confidence) of the fitting.

At higher $n_r \sim 0.9$, an additional heat capacity peak emerges near 1.5 K, which can be attributed to the appearance of a second layer commensurate solid phase (C2) analogous to ³He films on graphite [21]. However, the existence and exact symmetry of the C2 phase are still questionable, as numerical studies do not converge into a single conclusion [12,23,24,40]. Above $n_r \sim 0.9$, the heat capacity peak is slowly replaced by a sharp peak near 1 K due to an incommensurate solid phase (IC). The superfluid phase coexists with the C2 phase in a narrow coverage region near $n_r \sim 0.9$. We note that the uncertainty is $\delta n_r < 0.01$, smaller than the range of coexistence.

The phase diagram proposed here is consistent with recent diffusive Monte Carlo (DMC) calculations [24]. According to this work, the second layer undergoes a first-order phase transition from a low-density liquid into a 7/12 registered solid, stable within 18.2–18.6 atoms/nm². Above this coverage, an incommensurate triangular solid takes over near the layer completion. $\rho_s(T \rightarrow 0)$ in the low-density liquid region was estimated to be nearly 1, whereas it had a partially suppressed value in the 7/12 registered solid. In this reference, the incommensurate solid phase does not support superfluidity. This result can explain the suppression of the superfluidity initiated near the structural transition as well as the absence of superfluidity in the incommensurate solid phase that is observed here. Furthermore, the DMC calculation found a hexatic density correlation induced by a corrugation of the first layer in the liquid region [24], implying that the superfluid order is spatially modulated.

The coexistence of superfluid and solid orders was also confirmed by the DMC calculation [24]. ρ_s is rapidly suppressed inside the C2 phase, indicating competition between two orders tuned by n . One question naturally arises here: How do they coexist in the second layer? The

most intriguing answer is as a supersolid phase in which the superfluid and solid order coexist spontaneously in a single uniform state. Its possible observation was first reported by TO experiments with bulk solid ⁴He but was later attributed to the viscoelastic property change [41–43]. The supersolid phase has also been intensively studied in spatially ordered dipolar gas [44–46]. In addition, recent observations of a softening of excitation spectra that lead to the development of roton minima have been interpreted as the signature of supersolidity [47,48]. Although a perfect ⁴He single crystal might not be supersolid [49,50], this phase has proven to exist in Bosonic triangular lattices [51,52]. Otherwise, an alternative explanation for the coexistence is that certain region are phase-separated by forming domains with short-range density correlation. In this case, the superfluid occupies the area between the solid domains, but its percolation gets weaker as more ⁴He atoms are added. If n reaches some critical value where the registered solid does not support superfluid percolation, the superfluid disappears.

The spatially modulated superfluid phase observed here is a prime example of an exotic quantum phase resulting from the interplay among competing orders. Similarly, spatially modulated superconducting (SC) states have been widely explored in quantum materials where the d -wave SC state is coupled to the magnetic order [7,8] and forms the Fulde-Ferrell-Larkin-Ovchinnikov state in high magnetic fields [53]. In cuprate materials, the putative pair-density-wave (PDW) state, which is a spatially modulated SC order intertwined with spin- and charge-density-wave orders, has been suggested as a “mother” state when an SC order strongly competes with them [1]. Other descendant orders are “secondary” orders, generated by sequential symmetry breaking of the PDW state. Despite possible signatures from recent STM works [54,55], the observation

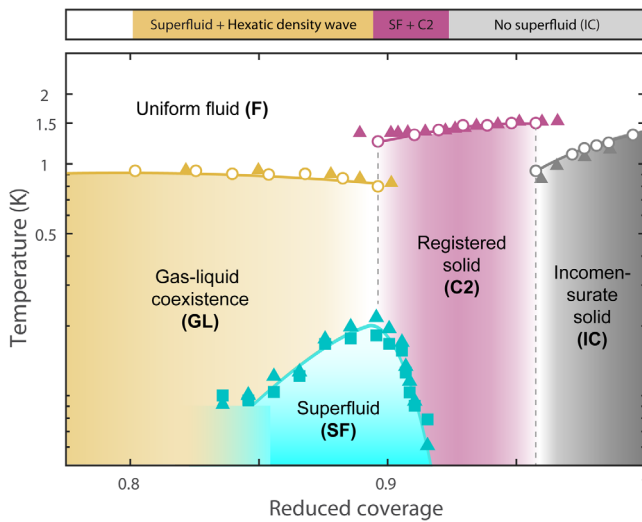


FIG. 4. Phase diagram of the second layer of ^4He films. T_s from this work (cyan) and the temperature of heat capacity loci (open circles and solid triangles) are plotted against reduced coverage (see text) with $n_2 = 21.2$ atoms/nm 2 [20,21]. A theoretical phase diagram [24] is drawn above the figure for comparison under the assumption of $n_2 = 20.4$ atoms/nm 2 . The uncertainty of n_r is smaller than 0.01.

of this long-sought PDW state has been hindered by the intrinsic complexity of strongly correlated systems. The exotic superfluid phases observed here and the recent searches for the PDW state in ^3He [56,57] imply that low-dimensional helium can provide excellent experimental platforms to realize novel quantum many-body phenomena for both bosons (^4He) and fermions (^3He), benefiting from their extremely pristine quality and reduced complexity [58].

In summary, our rigid two-frequency TO study of ^4He films on graphite provides unequivocal evidence of the superfluid phase in the second layer confined to a coverage range of 17–18.8 atoms/nm 2 . $\rho_s(T, n)$ measured at two frequencies were almost identical, indicating the existence of genuine superfluidity. Based on an accurate coverage measurement, a refined phase diagram of the second layer was presented. The superfluidity first emerges in the low-density liquid where the previous DMC calculations reported a superfluid ground state with a hexatic density-wave correlation. The superfluid state persists up to a higher coverage where the registered solid phase emerges. The coexistence of superfluid and solid orders leads to strong suppression of ρ_s , revealing a competing relationship between them. This exotic superfluid state intertwined with a structural order can be understood with an analogy to the spatially modulated superconducting state predicted in quantum materials where interplay among various competing orders plays a central role. This result suggests two-dimensional ^4He films as a model system for studying the interplay among broken-symmetry phases and for exploring exotic quantum ground states.

This work was supported by the National Research Foundation of Korea grant funded by the Korean government (MSIT) through MMO (2019R1A2C1009299) and the Center for Quantum Coherence in Condensed Matter (2016R1A5A1008184). J. C. especially thanks the POSCO TJ Park Foundation for its financial support through the TJ Park Science Fellowship.

*Corresponding author.
eunseong@kaist.edu

[†]Present address: Diamond Light Source, Ltd., Harwell Science and Innovation Campus, Didcot, Oxfordshire OX11 0DE, United Kingdom.

[‡]Present address: Quantum Dynamics Unit, Okinawa Institute of Science and Technology (OIST), 1919-1 Tancha, Okinawa 904-0495, Japan.

[§]These authors contributed equally to this work.

- [1] E. Fradkin, S. A. Kivelson, and J. M. Tranquada, Theory of intertwined orders in high temperature superconductors, *Rev. Mod. Phys.* **87**, 457 (2015).
- [2] J. C. S. Davis and D. H. Lee, Concepts relating magnetic interactions, intertwined electronic orders, and strongly correlated superconductivity, *Proc. Natl. Acad. Sci. U.S.A.* **110**, 17623 (2013).
- [3] R. M. Fernandez, P. P. Orth, and J. Schmalian, Intertwined vestigial order in quantum materials: Nematicity and beyond, *Annu. Rev. Condens. Matter Phys.* **10**, 133 (2019).
- [4] B. Keimer, S. A. Kivelson, M. R. Norman, S. Uchida, and J. Zaanen, From quantum matter to high-temperature superconductivity in copper oxides, *Nature (London)* **518**, 179 (2015).
- [5] D. F. Agterberg, J. C. S. Davis, S. D. Edkins, E. Fradkin, D. J. Van Harlingen, S. A. Kivelson, P. A. Lee, L. Radzihovsky, J. M. Tranquada, and Y. Wang, The physics of pair-density waves: Cuprate superconductors and beyond, *Annu. Rev. Condens. Matter Phys.* **11**, 231 (2020).
- [6] J. Chang, E. Blackburn, A. T. Holmes, N. B. Christensen, J. Larsen, J. Mesot, R. Liang, D. A. Bonn, W. N. Hardy, A. Watenphul, M. v. Zimmermann, E. M. Forgan, and S. M. Hayden, Direct observation of competition between superconductivity and charge density wave order in $\text{YBa}_2\text{Cu}_3\text{O}_{6.67}$, *Nat. Phys.* **8**, 871 (2012).
- [7] S. Gerber, M. Bartkowiak, J. L. Gavilano, E. Ressouche, N. Egetenmeyer, C. Niedermayer, A. D. Bianchi, R. Movshovich, E. D. Bauer, J. D. Thompson, and M. Kenzelmann, Switching of magnetic domains reveals spatially inhomogeneous superconductivity, *Nat. Phys.* **10**, 126 (2014).
- [8] D. Y. Kim, S. Z. Lin, F. Weickert, M. Kenzelmann, E. D. Bauer, F. Ronning, J. D. Thompson, and R. Movshovich, Intertwined Orders in Heavy-Fermion Superconductor CeCoIn_5 , *Phys. Rev. X* **6**, 041059 (2016).
- [9] S. Haddad, S. Charfi-Kaddour, C. Nickel, M. Héritier, and R. Bennaceur, Competing Phases in the High Field Phase Diagram of $(\text{TMTSF})_2\text{ClO}_4$, *Phys. Rev. Lett.* **89**, 087001 (2002).
- [10] H. F. Zhai, W. H. Jiao, Y. L. Sun, J. K. Bao, H. Jiang, X. J. Yang, Z. T. Tang, Q. Tao, X. F. Xu, Y. K. Li, C. Cao, J. H. Dai, Z. A. Xu, and G. H. Cao, Superconductivity, charge-

- spin-density wave, and metal-nonmetal transition in $\text{BaTi}_2(\text{Sb}_{1-x}\text{Bi}_x)_2\text{O}$, *Phys. Rev. B* **87**, 100502(R) (2013).
- [11] M. M. Ugeda, A. J. Bradley, Y. Zhang, S. Onishi, Y. Chen, W. Ruan, C. Ojeda-Aristizabal, H. Ryu, M. T. Edmonds, H. Z. Tsai, A. Riss, S. K. Mo, D. Lee, A. Zettl, Z. Hussain, Z. X. Shen, and M. F. Crommie, Characterization of collective ground states in single-layer NbSe_2 , *Nat. Phys.* **12**, 92 (2016).
- [12] P. Corboz, M. Boninsegni, L. Pollet, and M. Troyer, Phase diagram of ^4He adsorbed on graphite, *Phys. Rev. B* **78**, 245414 (2008).
- [13] M. C. Gordillo and J. Boronat, ^4He on a Single Graphene Sheet, *Phys. Rev. Lett.* **102**, 085303 (2009).
- [14] V. L. Berezinskii, Destruction of long-range order in one-dimensional and two-dimensional systems possessing a continuous symmetry group. ii. quantum systems, *Sov. Phys.-JETP* **34**, 610 (1972).
- [15] J. M. Kosterlitz and D. J. Thouless, Ordering, metastability and phase transitions in two-dimensional systems, *J. Phys. C* **6**, 1181 (1973).
- [16] P. A. Crowell and J. D. Reppy, Superfluidity and film structures in ^4He adsorbed on graphite, *Phys. Rev. B* **53**, 2701 (1996).
- [17] P. A. Crowell and J. D. Reppy, Reentrant Superfluid in ^4He Films Adsorbed on Graphite, *Phys. Rev. Lett.* **70**, 3291 (1993).
- [18] J. Nyéki, A. Phillis, A. Ho, D. Lee, P. Coleman, J. Parpia, B. Cowan, and J. Saunders, Intertwined superfluid and density wave order in two-dimensional ^4He , *Nat. Phys.* **13**, 455 (2017).
- [19] D. S. Greywall and P. A. Busch, Heat Capacity of Fluid Monolayers of ^4He , *Phys. Rev. Lett.* **67**, 3535 (1991).
- [20] D. S. Greywall, Heat capacity and the commensurate-incommensurate transition of ^4He adsorbed on graphite, *Phys. Rev. B* **47**, 309 (1993).
- [21] S. Nakamura, K. Matsui, T. Matsui, and H. Fukuyama, Possible quantum liquid crystal phases of helium monolayers, *Phys. Rev. B* **94**, 180501(R) (2016).
- [22] M. Pierce and E. Manousakis, Phase Diagram of Second Layer of ^4He Adsorbed on Graphite, *Phys. Rev. Lett.* **81**, 156 (1998).
- [23] J. Ahn, H. Lee, and Y. Kwon, Prediction of stable $\text{C}_{7/12}$ and metastable $\text{C}_{4/7}$ commensurate solid phases for ^4He on graphite, *Phys. Rev. B* **93**, 064511 (2016).
- [24] M. C. Gordillo and J. Boronat, Superfluid and Supersolid Phases of ^4He on the Second Layer of Graphite, *Phys. Rev. Lett.* **124**, 205301 (2020).
- [25] S. Lieu, A. F. Ho, D. K. K. Lee, and P. Coleman, Intertwined superfluid and density wave order in p -orbital Bose condensate, *Phys. Rev. B* **99**, 014504 (2019).
- [26] J. D. Reppy, X. Mi, A. Justin, and E. J. Mueller, Interpreting torsional oscillator measurements: Effect of shear modulus and supersolidity, *J. Low Temp. Phys.* **168**, 175 (2012).
- [27] M. H. W. Chan, A. D. Migone, K. D. Miner, and Z. R. Li, Thermodynamic study of phase transitions of monolayer N_2 on graphite, *Phys. Rev. B* **30**, 2681 (1984).
- [28] G. Zimmerli, G. Mistura, and M. H. W. Chan, Third-Sound Study of a Layered Superfluid Helium, *Phys. Rev. Lett.* **68**, 60 (1992).
- [29] A. Noury, J. Vergara-Cruz, P. Morfin, B. Plaçais, M. C. Gordillo, J. Boronat, S. Balibar, and A. Bachtold, Layering Transition in Superfluid Helium Adsorbed on a Carbon Nanotube Mechanical Resonator, *Phys. Rev. Lett.* **122**, 165301 (2019).
- [30] See Supplemental Material at <http://link.aps.org/supplemental/10.1103/PhysRevLett.127.135301> for other experimental details including the design of a rigid two-frequency TO, and for measurements on the third layer.
- [31] J. Day and J. Beamish, Low temperature shear modulus changes in solid ^4He and connection to supersolidity, *Nature (London)* **450**, 853 (2007).
- [32] M. Hieda, T. Nishino, M. Suzuki, N. Wada, and K. Torii, Slippage of Nonsuperfluid Helium Films, *Phys. Rev. Lett.* **85**, 5142 (2000).
- [33] N. Hosomi and M. Suzuki, Sliding friction of multilayer ^4He films adsorbed on graphite, *Phys. Rev. B* **77**, 024501 (2008).
- [34] M. H. W. Chan, K. I. Blum, S. Q. Murphy, G. K. S. Wong, and J. D. Reppy, Disorder and the Superfluid Transition in Liquid ^4He , *Phys. Rev. Lett.* **61**, 1950 (1988).
- [35] J. Choi, J. Shin, and E. Kim, Frequency-dependent study of solid ^4He contained in a rigid double-torus torsional oscillator, *Phys. Rev. B* **92**, 144505 (2015).
- [36] J. Choi, T. Tsuiki, D. Takahashi, H. Choi, K. Kono, K. Shirahama, and E. Kim, Reinvestigation of the rotation effect in solid ^4He with a rigid torsional oscillator, *Phys. Rev. B* **98**, 014509 (2018).
- [37] G. Agnolet, D. F. McQueeney, and J. D. Reppy, Kosterlitz-Thouless transition in helium films, *Phys. Rev. B* **39**, 8934 (1989).
- [38] D. J. Bishop and J. D. Reppy, Study of the superfluid transition in two-dimensional ^4He films, *Phys. Rev. B* **22**, 5171 (1980).
- [39] G. A. Csáthy, J. D. Reppy, and M. H. W. Chan, Substrate-Tuned Boson Localization in Superfluid ^4He Films, *Phys. Rev. Lett.* **91**, 235301 (2003).
- [40] S. Moroni and M. Boninsegni, Second-layer crystalline phase of helium films on graphite, *Phys. Rev. B* **99**, 195441 (2019).
- [41] E. Kim and M. H. W. Chan, Probable observation of a supersolid helium phase, *Nature (London)* **427**, 225 (2004).
- [42] E. Kim and M. H. W. Chan, Observation of superfluid in solid helium, *Science* **305**, 1941 (2004).
- [43] J. Beamish and S. Balibar, Mechanical behavior of solid helium: Elasticity, plasticity, and defects, *Rev. Mod. Phys.* **92**, 045002 (2020).
- [44] J. Léonard, A. Morales, P. Zupancic, T. Donner, and T. Esslinger, Monitoring and manipulating Higgs and Goldstone modes in a supersolid quantum gas, *Science* **358**, 1415 (2017).
- [45] J. Léonard, A. Morales, P. Zupancic, T. Donner, and T. Esslinger, Supersolid formation in a quantum gas breaking a continuous translational symmetry, *Nature (London)* **543**, 87 (2017).
- [46] J. R. Li, J. Lee, W. Huang, S. Burchesky, B. Shteynas, F. C. Top, A. O. Jamison, and W. Ketterle, A stripe phase with supersolid properties in spin-orbit-coupled Bose-Einstein condensates, *Nature (London)* **543**, 91 (2017).
- [47] D. Petter, G. Natale, R. M. W. van Bijnen, A. Patscheider, M. J. Mark, L. Chomaz, and F. Ferlaino, Probing the Roton

- Excitation Spectrum of a Stable Dipolar Bose Gas, *Phys. Rev. Lett.* **122**, 183401 (2019).
- [48] G. Natale, R. M. W. van Bijnen, A. Patscheider, D. Petter, M. J. Mark, L. Chomaz, and F. Ferlaino, Excitation Spectrum of a Trapped Dipolar Supersolid and Its Experimental Evidence, *Phys. Rev. Lett.* **123**, 050402 (2019).
- [49] N. Prokof'ev and B. Svistunov, Supersolid State of Matter, *Phys. Rev. Lett.* **94**, 155302 (2005).
- [50] M. Boninsegni, N. Prokof'ev, and B. Svistunov, Superglass Phase of ^4He , *Phys. Rev. Lett.* **96**, 105301 (2006).
- [51] M. Boninsegni and N. Prokof'ev, Supersolid Phase of Hard-Core Bosons on a Triangular Lattice, *Phys. Rev. Lett.* **95**, 237204 (2005).
- [52] S. Wessel and M. Troyer, Supersolid Hard-Core Bosons on the Triangular Lattice, *Phys. Rev. Lett.* **95**, 127205 (2005).
- [53] Y. Matsuda and H. Shimahara, Fulde-Ferrell-Larkin-Ovchinnikov state in heavy-fermion superconductors, *J. Phys. Soc. Jpn.* **76**, 051005 (2007).
- [54] Z. Du, H. Li, S. H. Joo, E. P. Donoway, J. Lee, J. C. S. Davis, G. Gu, P. D. Johson, and K. Fujita, Imaging the energy gap modulations of the cuprate pair-density-wave state, *Nature (London)* **580**, 65 (2020).
- [55] P. Choubey, S. H. Joo, K. Fujita, Z. Du, S. D. Edkins, M. H. Hamidian, H. Eisaki, S. Uchida, A. P. Mackenzie, J. Lee, J. C. S. Davis, and P. J. Hirschfeld, Atomic-scale electronic structure of the cuprate pair density wave state coexisting with superconductivity, *Proc. Natl. Acad. Sci. U.S.A.* **117**, 14805 (2020).
- [56] L. V. Levitin, B. Yager, L. Sumner, B. Cowan, A. J. Casey, J. Saunders, N. Zhelev, R. G. Bennett, and J. M. Parpia, Evidence for a Spatially Modulated Superfluid Phase of ^3He Under Confinement, *Phys. Rev. Lett.* **122**, 085301 (2019).
- [57] A. J. Shook, V. Vadakkumbatt, P. S. Yapa, C. Doolin, R. Boyack, P. H. Kim, G. G. Popowich, F. Souris, H. Christani, J. Maciejko, and J. P. Davis, Stabilized Pair Density Wave Via Nanoscale Confinement of Superfluid ^3He , *Phys. Rev. Lett.* **124**, 015301 (2020).
- [58] J. Saunders, B. Cowan, and J. Nyéki, Atomically layered helium films at ultralow temperatures: Model systems for realizing quantum materials, *J. Low Temp. Phys.* **201**, 615 (2020).